Particle image velocimetry measurement inside axial air test turbine – Effect of window

Cite as: AIP Conference Proceedings **2323**, 030005 (2021); https://doi.org/10.1063/5.0041492
Published Online: 08 March 2021

Daniel Duda, Tomáš Jelínek, Martin Němec, Václav Uruba, Vitalii Yanovych, and Pavel Žitek

Particle Image Velocimetry Measurement inside Axial Air Test Turbine – Effect of Window

Daniel Duda[1, a)], Tomáš Jelínek[2, b)], Martin Němec[2, c)], Václav Uruba[1, 3, d)], Vitalii Yanovych[1, e)] and Pavel Žitek[1, b, f)]

[1]*University of West Bohemia in Pilsen, Univerzitní 22, Pilsen, Czech Republic.*
[2]*Czech Aerospace Research Centre, Ke Kouli 2, Prague, Czech Republic.*
[3]*Institute of Thermomechanics, Czech Academy of Sciences, Dolejškova 5, Prague, Czech Republic.*

[a)]Corresponding author: dudad@kke.zcu.cz
[b)]jelinek@vzlu.cz
[c)]nemec@vzlu.cz
[d)]uruba@kke.zcu.cz
[e)]yanovichvitaliy@i.ua
[f)]zitek@kke.zcu.cz

Abstract. We measure the two dimensional instantaneous velocity fields inside an axial turbine by using the technique PIV (Particle Image Velocimetry). The measured plane is located just behind the rotor wheel and it is oriented in axial × tangential direction. We measured a single overloaded regime as well as the nominal one at tip radius. We discuss several technical difficulties appearing during this measurement, mainly with the seeding particles and with the optical access into a massive steel body. The glass dividing the channel past rotor and the empty space of diffusor has been dirtied by large oil droplets condensing at the blades and splashed to this window. We "solved" this trouble by removing the glass, because it anyway divides volumes with same static pressure. Best quality result was obtained without this glass, but its removal changes the geometry. In our contribution we focus to the effect of such rude change to the trustworthiness of the results.

INTRODUCTION

Among the variety of methods for measuring flow velocity, the technique of Particle Image Velocimetry (PIV) [1] offers the *spatial resolution* of the instantaneous velocity field, which is advantageous for studying the coherent structures of turbulence. The ensemble of such instantaneous velocity fields serves for both, the studies of the average flow pattern as well as for the fluctuation structures of Reynolds decomposed velocity fields [2]. PIV is an optical method, therefore it does not disturb the flow by any probe, but on the other hand, it needs seeding particles, whose motion is measured. The need of optical access from two directions (for illumination laser and for camera) makes its use difficult for in-situ measurements. Another disadvantage is the slow laser charging limiting the temporal resolution far under the typical time of the flow. This disadvantage can be partly canceled by the synchronization of the PIV system with the rotation the rotor, which results into set of instantaneous velocity fields, which are not correlated in time, but in the phase of the periodically driven flow.

This is the reason, why the majority of engineering hydrodynamic studies are performed by using pressure probes [1], whose robustness and quite straightforward interpretation (only the knowledge of fluid density is needed) make them the first choice for in-situ testing. But, the pressure probe needs to be pointed directly against the main flow and, when the angle is not known or it is a subject of investigation, then a multihole probe with quite complicated calibration procedure has to be used.

19th Conference on Power System Engineering
AIP Conf. Proc. 2323, 030005-1–030005-12; https://doi.org/10.1063/5.0041492
Published by AIP Publishing. 978-0-7354-4067-8/$30.00

There exist more of the so-called point methods (it does not refer to the fluid point, with size smaller than Kolmogorov length, but to the fact, that their results have form of a single number representing the entire probed volume) with or without the temporal resolution. The above mentioned pressure probes typically do not offer the fine temporal resolution, only when the pressure transducer is very close to the hole. The imaginary "king" in the time resolution is the Hot Wire Anemometry method (sometimes referred as Constant Temperature Anemometry) [1], with sampling frequency going into hundreds of kilohertz. On the other hand, the wire itself is very fragile and has a limited lifetime. The turbomachinery hydrodynamics is mostly studied by pressure methods; deeper studies use Hot Wire Anemometry [3].

EXPERIMENTAL SETUP

The test facility at the Czech Aerospace Center consists of single stage axial air turbine, the hydraulic dynamometer and powerful 12-stages air compressor. This facility serves mainly for measuring integral characteristics of different rotor and stator wheels under large scale of conditions. While the measurement with pressure probes is quite common here, the optical methods need a new access into the turbine.

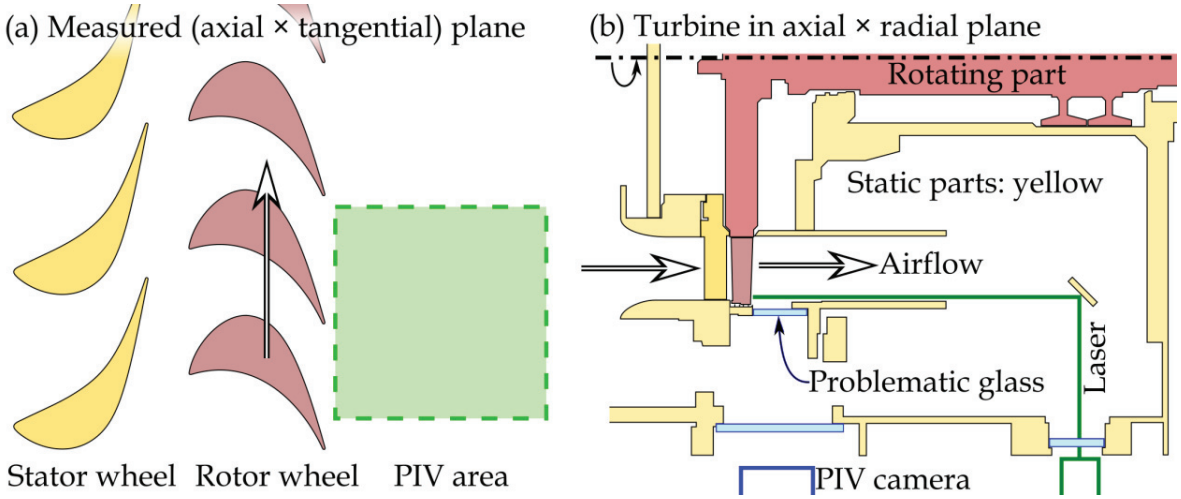

FIGURE 1. Left: sketch of the studied PIV area just behind the rotor wheel. The air flows from left to right. Right: sketch of the top view cut of the turbine. The air flows from left to right and then turns down into the exhaust.

The PIV (Particle Image Velocimetry) technique is based on observing the motion of small particles carried by the flow. These particles are illuminated by a double-pulsed solid state laser with beam defocused in one direction by a cylindrical lens (in fact it is more lenses) resulting into a planar laser-sheet of thickness about 1 mm and width in order of tens or hundreds of mm in dependence on distance from aperture. We use the NewWave Solo laser with pulse energy up to 500 mJ. The particle positions are captured by using a camera, which can distinguish two expositions separated by only few microseconds (5 μs in the present data). We use the Mk II FlowSense 4 MPix camera.

The optical access for laser beam is localized in the diffusor body by window in the cylindrical steel wall. The laser is oriented perpendicularly to the turbine axis and the laser sheet is mirrored into the counter-axial direction by using a planar mirror mounted on a computer-controlled linear traverser, which allow changing the explored radius. In this contribution we present only data taken at the tip radius.

The optical access for camera is made in the cylindrical body axially just behind the rotor wheel. There are two windows due to the presence of a cylindrical wall, which is a removable insert allowing installation of different size wheels into the test turbine.

The synchronization of PIV system and rotor wheel rotations allow to study the average pattern of the rotor wake. The instantaneous data show large amount of vortices of size about the shear layer thickness and the spatial spectrum follow the Kolmogorov scaling for homogeneous and isotropic turbulence under that size.

We had several troubles with the condensation of seeding particles on the glass between the diffuser and main body. Best quality result was obtained without this glass, but its removal changes the geometry. In our contribution we focus to the effect of such rude change to the trustworthiness of the results.

RESULTS – NOMINAL REGIME

Figure 2 shows the in-plane angle of average velocity in respect to the axial direction:

$$\alpha = \operatorname{atan}\frac{v}{u} \tag{1}$$

where u and v are the axial and tangential velocity components respectively. Note that there is important first to average, second to calculate the angle, as the atan function is non-linear, therefore averaging instantaneous angles gives different result than angle of average velocity.

The average flow pattern has a form of alternating approximately vertical strips faster and slower fluid (Fig. 3) corresponding to jets and wakes past the rotor wheel (wakes past the blades, jets past the inter-blade channels). In the shear layers between jets and wakes, the average flow direction is deflected in the tangential direction (Fig. 2). These strips are partially overlapped by horizontal wakes (~ upper half of field of view) and jets (~ bottom half of field of view) caused by the stator wheel preceding the rotor. We can see that the inhomogeneity of flow angle caused by rotor blades is less disturbed in the shear layer between the wake and jet of stator. The deflection of flow angle signifies the fluid still contain some momentum, which has not been transferred to the rotor and thus this energy is escaping the turbine. The spatial average and standard deviation of angle of (temporal) average velocity is -3.2° ± 4.8° for the case without glass, while it is -3.5° ± 4.5° with glass.

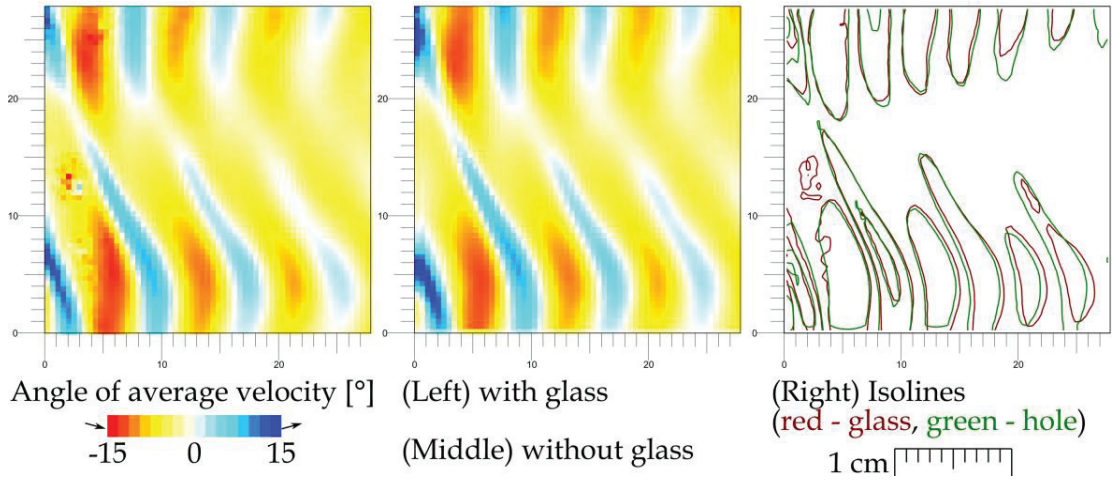

FIGURE 2. Angle of ensemble (600 snapshots) averaged velocity. The angle is relative to the axial direction. The data are taken at tip radius at Mach number Ma = 0.40 and under nominal conditions.

The inner glass closing the hole in the diffusor body causes serious troubles due to oil droplets decreasing transparency and causing spurious reflections. These reflections from large droplets slowly traveling on the glass are a big problem as they move and thus cannot be subtracted. Their effect is visible even in average data – see the left part of Fig. 2, where a spurious spot of differently oriented velocity shines. The higher moments are naturally even more sensitive to such disturbances.

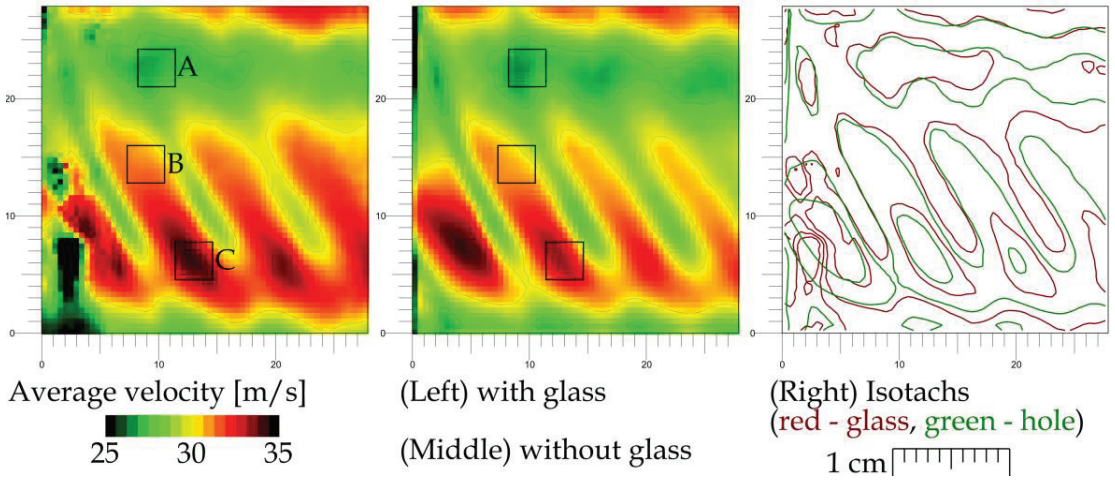

FIGURE 3. Magnitude of average velocity. The legend spans ± 5 m/s around the average magnitude (which is measured to be 29.9 and 29.5 m/s respectively). Black rectangles highlight cross-section of stator and rotor wake (A), that of stator and rotor jet (C) and the area of minimal turbulence (B); they will be discussed later. The data are taken at tip radius at Ma = 0.40 and under nominal conditions.

Due to the lack of measuring time during this quite complicated campaign, we "solved" this issue simply by removing the problematic part. The quality of resulting data is much better, as can be seen in Fig. 2 middle, but, on the other hand, it changes the geometry significantly! Fortunately, the static pressure on both sides of the inner body (which in fact only serves for fitting different radii wheels into the test facility) is same. Therefore, the flow might not be affected much. To answer this important question, we compare data at both variants in light of isolines (or contour lines) of several average quantities.

The magnitude w displayed in Fig. 3 is calculated by using the in-plane velocity components only (they are measured):

$$w = \sqrt{u^2 + v^2} \tag{2}$$

In this plot we can see the effect of widening of the flow path in the case with hole in the outer cylindrical body: the right parts of the fields of view display systematically lower velocity magnitude (greener colors) in the case with hole.

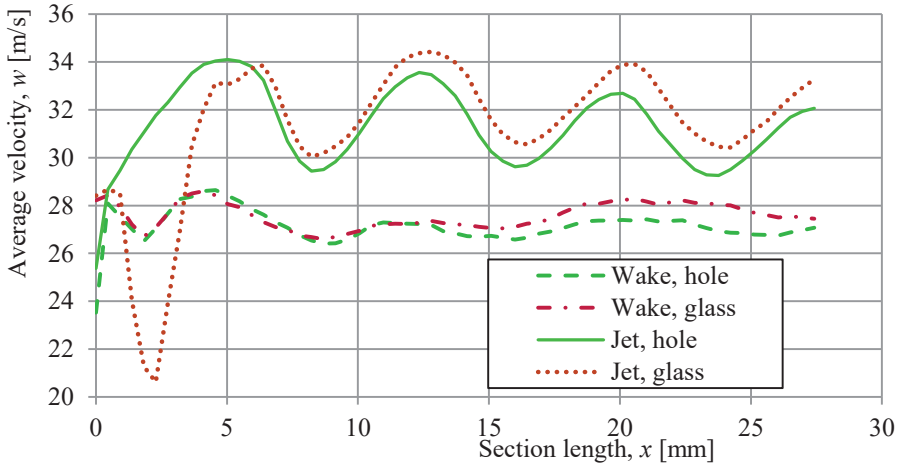

FIGURE 4. Magnitude of average velocity along axial sections following jet (y-position of C region) and wake (y-position of A region) respectively.

This effect is better apparent when comparing the sections of this data, see Fig. 4. Still, the effect of artificial hole in the outer cylindrical wall is smaller than the inhomogeneity of the velocity caused by the stator wheel. It is

interesting, that the height of velocity peaks associated with rotor system is larger in the stator jet, than in the stator wake.

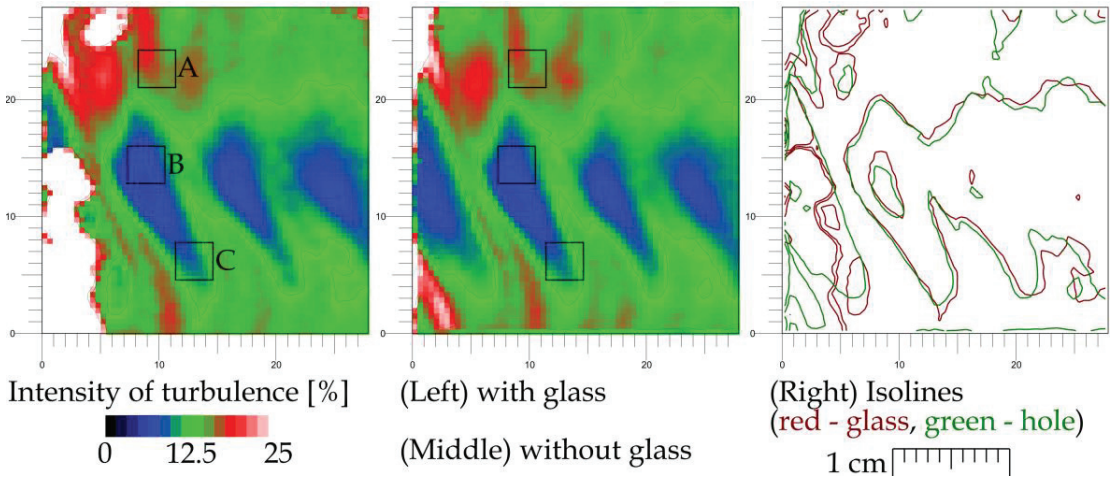

FIGURE 5. Turbulence intensity calculated by using the in-plane components (it is underestimated by the radial components and by the fluctuations of length-scale smaller than the experimental resolution). The data are taken at tip radius at Mach number Ma = 0.40 and under nominal conditions. Note the intense noise caused by the droplets in the case with glass.

The turbulence intensity is defined historically as the ratio of standard deviation of velocity to its average value

$$I_T = \frac{\sigma[u]}{\langle u \rangle} \tag{3}$$

but, we have to note, that this definition is prepared for typical one-dimensional point method with average drift velocity significantly larger than the fluctuations. PIV is not limited by this requirement and it is two-dimensional method. Thus we rather use the definition with energies, which for 1D case converge to the definition above:

$$I_T = \sqrt{\frac{\langle u^2 \rangle - \langle u \rangle^2 + \langle v^2 \rangle - \langle v \rangle^2}{\langle u \rangle^2 + \langle v \rangle^2}} \tag{4}$$

Turbulence intensity represents the amount of energy, which is already removed from the main flow, and it has the form of mechanical energy still, but with higher entropy – it occupies smaller length-scales and it is not organized regularly in time. An interesting question asks, in which direction the velocity fluctuates more [4]. It is generally known [5, 6], that in the case of wake flows, the stream-wise fluctuations are stronger in the shear layer at the wake boundary, but in the center of the wake, there dominate the span-wise fluctuations.

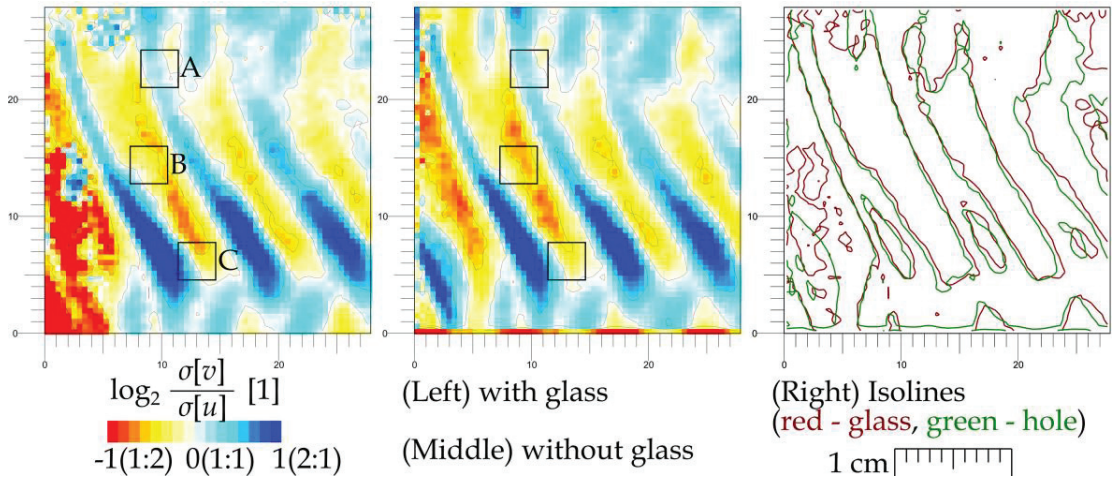

FIGURE 6. Anisotropy of fluctuations in light of ratio of fluctuations in the tangential to the axial direction [4]. Logarithm is advantageous for this quantity, because it maps the interval [0, ∞] with center in 1 (fluctuations same in both directions) to symmetric interval [-∞, ∞] with center in 0 (i.e. -∞ corresponds to all fluctuations in axial direction, +∞ does for all in tangential direction, -1 means that there is 2× more fluctuations in axial direction than in tangential one and +1 does oppositely).

Our findings according to 2D isotropy (for the full insight into the isotropy of fluctuations we would need the Stereo PIV data [7], which is planned for future) are shown in Fig. 6, where we compare the amount of fluctuations in tangential and axial direction. The topology of this ratio follows the spatial distribution of velocity angle (Fig. 2).

Statistics of Tangential Velocity

In Fig. 3 we depicted three regions of interest; first (A) lies in the cross-section of stator a rotor wakes, the magnitude of average velocity is minimal there; second (B) is area of minimal intensity of turbulence (compare with Fig. 3) and the third (C) displays maximum magnitude of average velocity. We show the statistics of tangential velocity component in these regions in Fig. 7. In the later figures, we show the spatial maps of first four statistical moments of the ensemble distribution in order to support the observations made from the full distribution display (Fig. 7), which can, for the clearance reasons, show only a small amount of interesting locations.

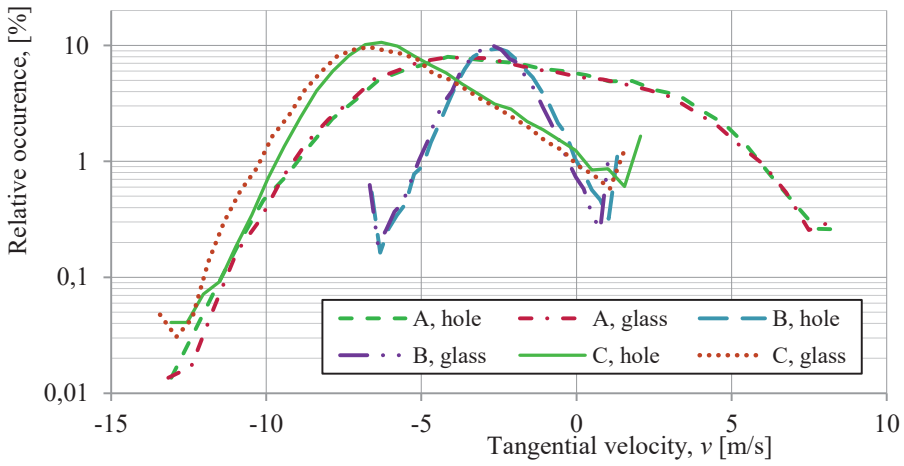

FIGURE 7. Histogram of instantaneous tangential velocity component in three depicted regions. The vertical axis is in logarithmic scale and it is normalized by the number of points; the horizontal axis is linear and not normalized in order to show different means as well. The first and last point of each line contains events out of the interval. Each line contains 29400 datapoints.

We see, that the A area of lowest velocity magnitude (which we believe to be associated of the cross-section of stator and rotor wake) has largest variance of the tangential velocity component; additionally, the distribution is asymmetric with larger probability at the slightly negative values. The area B (selected in the minimum of turbulence intensity) displays rather normal distribution with symmetrically decreasing tails. The area C at the highest velocity magnitude contains very asymmetric distribution of events. The shape of distributions seems to be only little affected by the presence of the glass. Largest discrepancy occurs at the C area, where there is slightly larger amount of stronger events with glass than without glass. This issue could have two reasons: (i) the optical noise of droplets, or (ii) it can have a physical reason – the stronger events could be attenuated by the presence of hole in the wall.

Tangential velocity component is important from the energetic point of view, because it carries out the angular momentum, which cannot be used as a turbine work. Inside a mysterious ideal turbine, the outgoing tangential velocity might be zero at all positions and at all times.

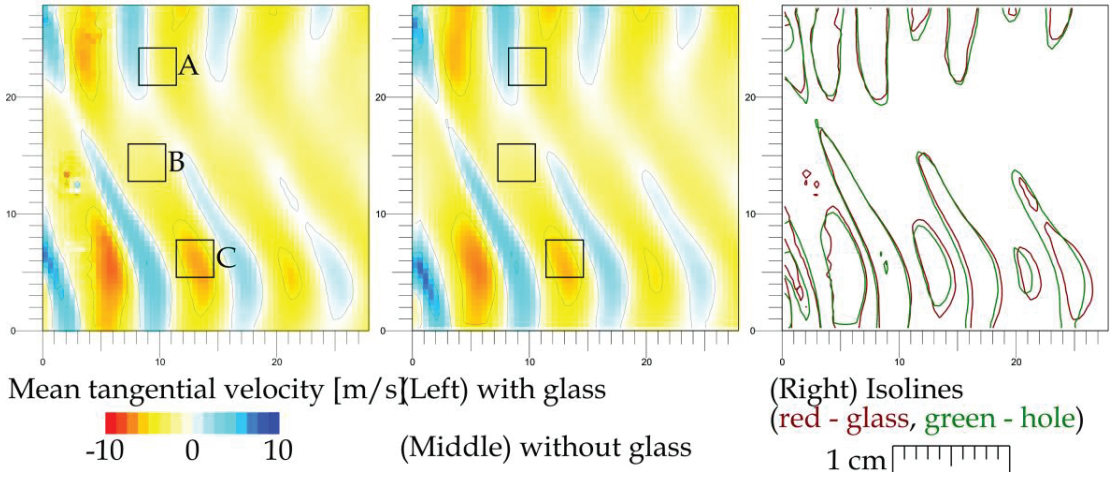

FIGURE 8. First statistical moment (i.e. average) of tangential velocity v.

The first statistical moment is just an ensemble average. Its topology is very similar to that of angle of average velocity (compare Figs 8 and 2).

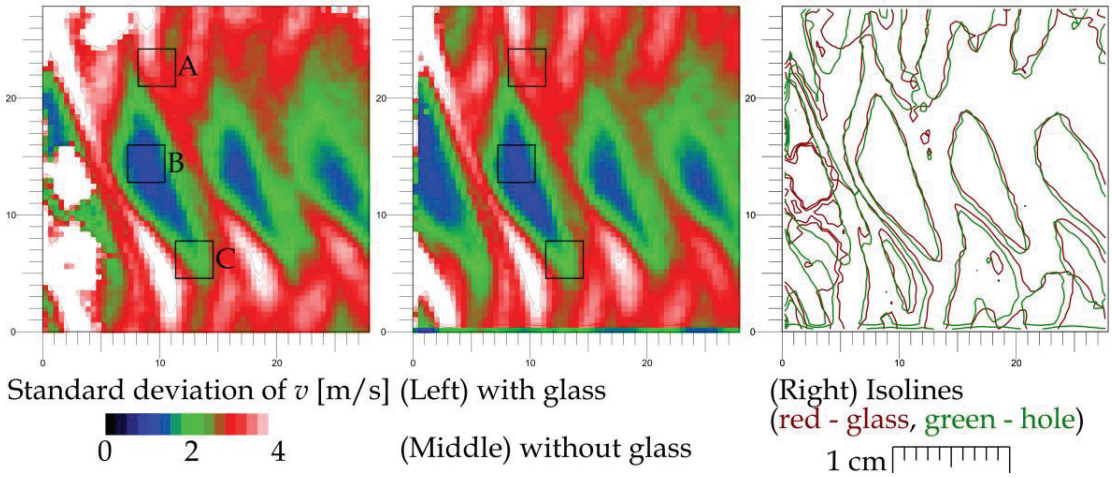

FIGURE 9. Second statistical moment (i.e. standard deviation) of tangential velocity v.

The second statistical moment is called standard deviation σ and it is calculated as

$$\sigma[v] = \langle (v - \langle v \rangle)^2 \rangle = \langle v^2 \rangle - \langle v \rangle^2 \tag{5}$$

Its pattern is very similar to that of turbulence intensity (Fig. 5), because turbulence intensity consists partly of this quantity and, at the same time, the ratio of axial and tangential fluctuations does not depart much from isotropy (see Fig. 6).

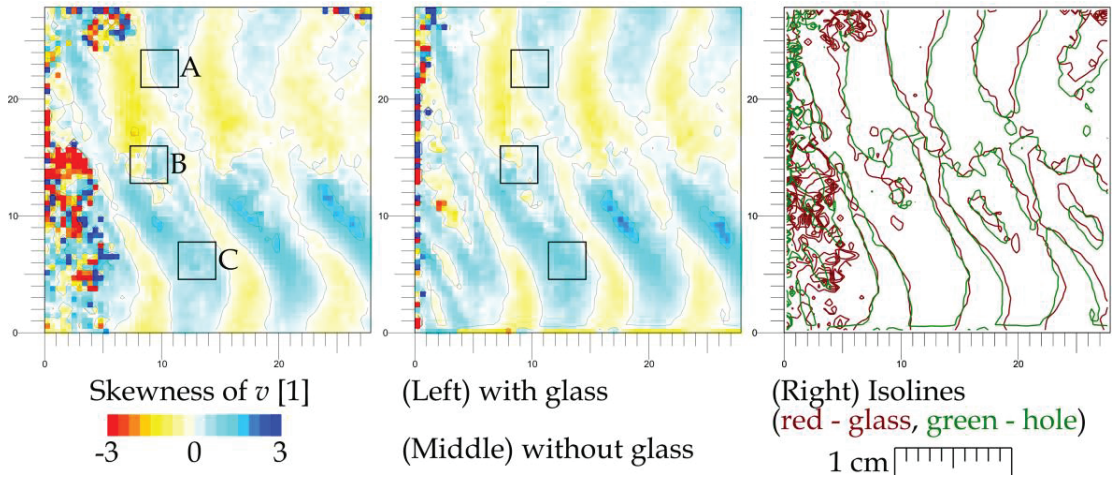

FIGURE 10. Third statistical moment (i.e. skewness) of tangential velocity v.

The third statistical moment, called *skewness*, shows the left-right anisotropy of strong rare events. In other words, the negative skewness tells, that there are few events much smaller than the mean, which are balanced by higher number of events not so larger than the mean. Positive value means oppositely. Skewness is calculated as

$$S[v] = \frac{\langle (v - \langle v \rangle)^3 \rangle}{\sigma^3[v]} \tag{6}$$

therefore, it is a dimensionless quantity. As the moment rises, the result is much more sensitive to the noise (it focuses to rare events far from average), thus also the plot of S is less visually attractive than some mean quantities. This phenomenon is much stronger for the Flatness making this quantity difficult to use to some tough physical conclusions.

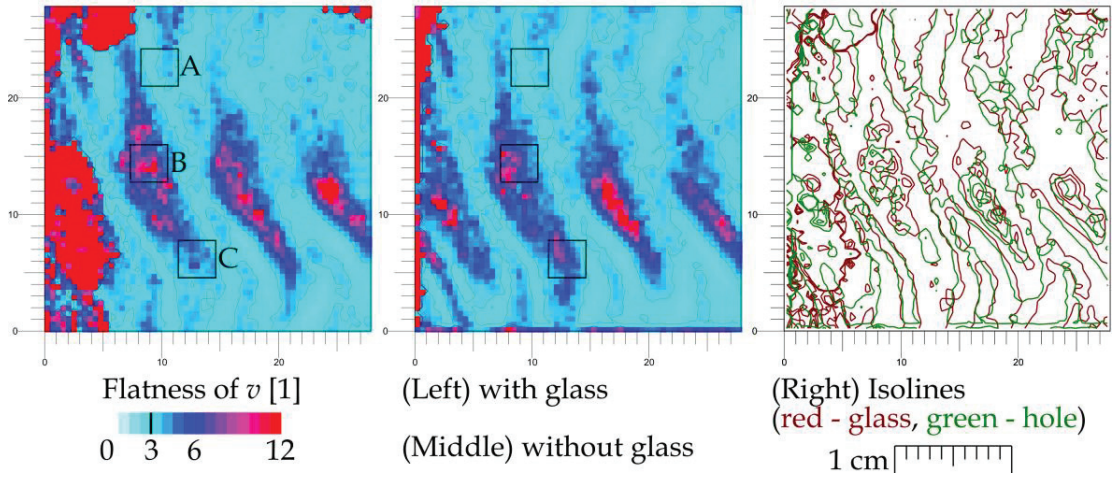

FIGURE 11. Forth statistical moment (i.e. flatness) of tangential velocity v. Flatness of a Gaussian distribution is equal to 3, which is depicted in the legend and it is the level of one isoline.

Flatness is the fourth statistical moment calculated as

$$F[v] = \frac{\langle (v - \langle v \rangle)^4 \rangle}{\sigma^4[v]} \tag{7}$$

it is very sensitive to strong rare events (and naturally to the noise as well). Physically, it is interpreted as a sign of intermittency. It is typically produced in the areas with generally quiet flow, which are time-to-time visited by a turbulent patch from the neighboring wilder regions; therefore, it is large in the areas, where turbulence intensity is smaller. Look to region B, where F is high, while σ is low. Similarly, in the histogram plot (Fig. 7), region B displays narrow distribution with high out-of-interval peaks.

Overloaded Regime

The off-design regimes are very important in nowadays, when the instability caused by so-called green energy resources has to be compensated in classical steam turbines, which are then forced to work during significant periods in off-design regimes.

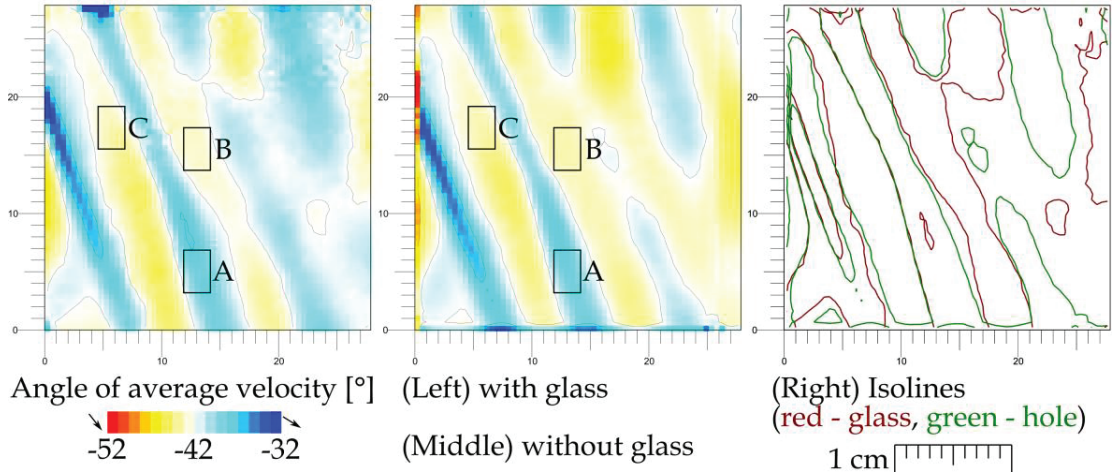

FIGURE 12. Angle of average velocity. The data are taken at tip radius at Mach number Ma = 0.40 and at overloaded regime with wheel-to-fluid ratio 0.40.

The overloaded regime occurs when the breaking force acting to the rotor wheel slows its velocity under the ideal one; direct consequence is the non-axial direction of fluid leaving the stage, which carries a relevant amount of axial momentum, i.e. energy which is not transferred to the mechanical energy of the rotor. In this measurement, we tested the overload regime with ratio of rotor speed to the axial fluid velocity equal to 0.4 (remember this ratio at nominal regime was 0.55).

The measured spatial average of angle of ensemble-average fluid velocity is -41.3° ± 2.2° with the problematic covering glass, or it is measured to be -42.0° ± 2.3° without this glass.

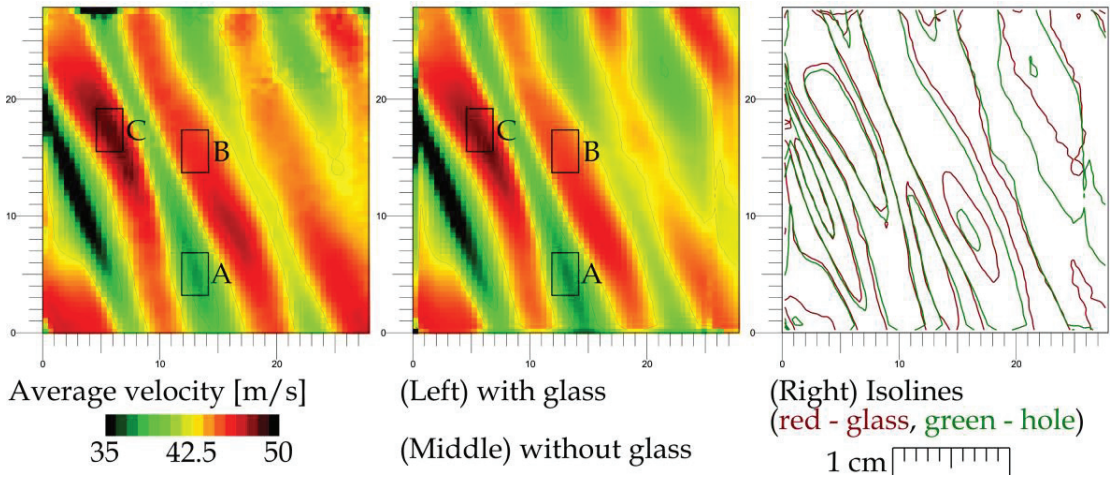

FIGURE 13. Magnitude of average velocity. The data are taken at tip radius at Mach number Ma = 0.40 and at overloaded regime with wheel-to-fluid ratio 0.40.

The topology, again, consists of system of wakes and jets past rotor wheel and a similar system past stator wheel, which is parallel with the average flow (stator is static). Therefore, the overlap regions of stator jet with rotor jet or stator wake with rotor wake are larger and thus they can contain larger turbulent structures. Larger structures contain more energy and therefore the energy dissipation is larger than under nominal conditions.

The overloaded regime is much more affected by the droplets splashed onto the window, which is most apparent at the distribution of higher moments, e.g. the turbulence intensity in Fig. 14. The quality of data is not high, thus we had to use a filtering algorithm based on the energy content at lowest resolved length scale described in our article [8]. On the other hand, the overloaded regime seems to be more sensitive to the geometry change caused by removing the glass leaving a hole in its place. This is logic, when we take into account the non-zero tangential motion of the fluid and the consecutive centrifugal force creating a positive pressure deviation at the boundary.

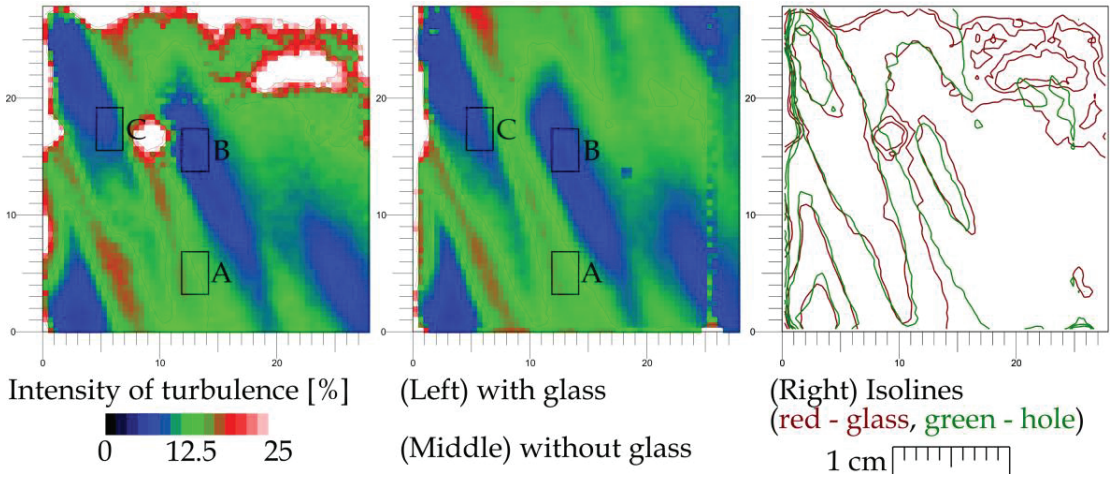

FIGURE 14. Turbulence intensity. Note the clearly apparent individual droplets apparent as spots of diverging I_T. The data are taken at tip radius at Mach number Ma = 0.40 and at overloaded regime with wheel-to-fluid ratio 0.40.

While the field of view was affected by the splashed droplets most in its left part under the nominal condition, at the overloaded regime, it contains more noise in its upper part – compare Figs 5 and 14 plotting the turbulence intensity.

The ratio of intensities of fluctuations in the tangential to that in the axial direction does not make sense in the areas disturbed by some droplets, but elsewhere it displays quite a good agreement between the two discussed cases as well as with the topology of the angle distribution, which has been argued previously.

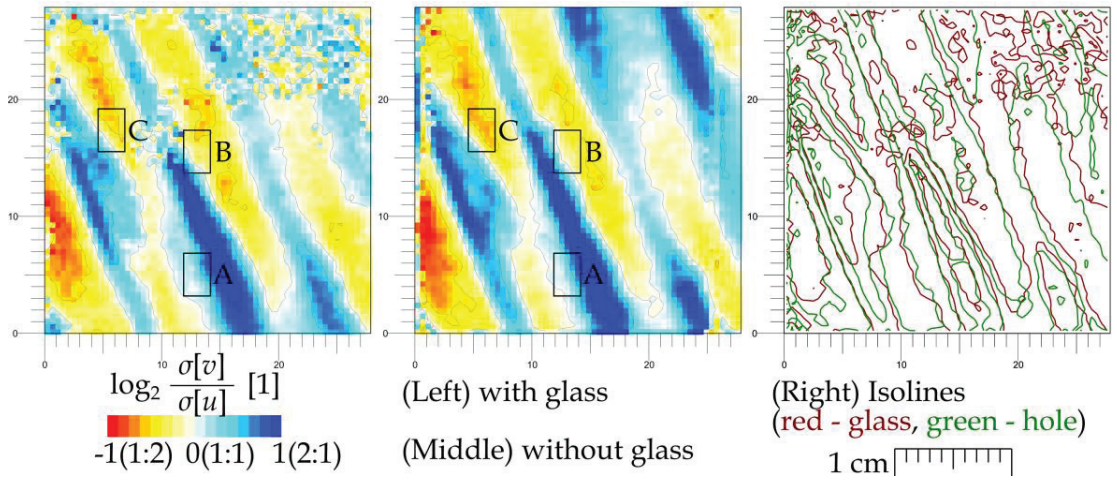

FIGURE 15. Anisotropy of fluctuations in light of ratio of fluctuations in the tangential to the axial direction [4]. Ignore the point noise in disturbed areas (white spots in previous Fig. 14). The data are taken at tip radius at Mach number Ma = 0.40 and at overloaded regime with wheel-to-fluid ratio 0.40.

We selected different regions of interest according to the same key as above. These regions are located at the lowest velocity magnitude (A), which can be interpreted as a cross-section point of wake past stator with wake past rotor; second is located at the minimum turbulence intensity (B), and the third one at the highest velocity magnitude (C), which we interpret as cross-section of stator and rotor jets. The distribution of tangential velocities at these regions is plotted in Fig. 16.

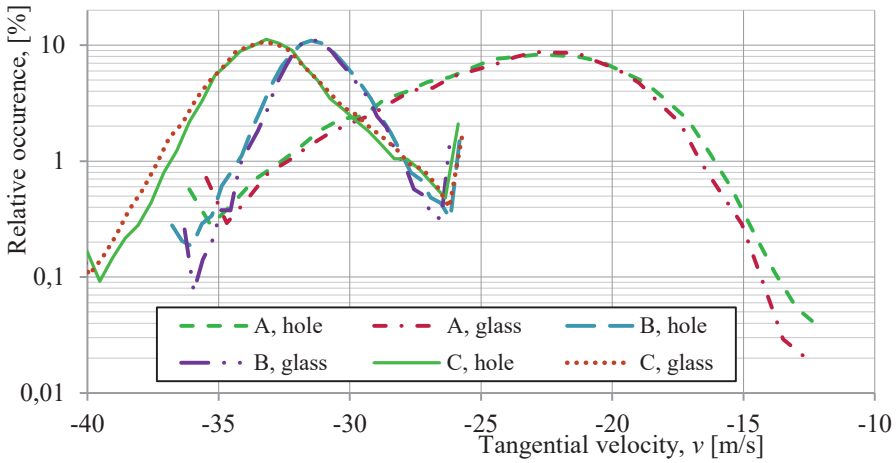

FIGURE 16. Histogram of instantaneous tangential velocities. The first and last point of each line contains events out of the interval. Datalines associated with glass contains 24000 datapoints, while that of hole consist of 23920 points.

The histogram of tangential velocity events in three depicted areas shows again, that the A-area in the cross-section of stator and rotor jet display a significant asymmetry as being spread to the stronger (downwards) events, while the decrease at the positive part (which is still negative) is much steeper. The regions B and C behave oppositely, with center at much more negative velocities (C is located in the maximum of velocity magnitude associated with the cross-section of stator and rotor jet, while B lies in the area of minimal turbulence intensity). The histograms display a very similar values between the cases with and without glass.

CONCLUSION

By using Particle Image Velocimetry technique, we studied the flow at the output of a single-stage axial turbine at the tip radius. There occurred troubles with oil droplets splashed on the glass window decreasing significantly the quality of data preventing any deeper analysis. We "solved" this problem by removing this problematic glass and in this contribution we show on the available data, that the error caused by this geometry change is more than redeemed by the increase of data quality. Higher discrepancy is observed in the magnitude of average velocity, while the turbulence statistics seem to be unaffected by this change.

ACKNOWLEDGMENTS

We thank to Bohumil Laštovka and Jakub Pokorný for valuable technical help with preparation of experiment.

We thank to Jan Uher and Petr Milčák from Doosan Škoda Power for valuable discussions preceding this measurement. We thank gratefully to Mária and Marek Richter and to Eva Berková for technical help with data transfer.

This work was supported by the project of Technology Agency of the Czech Republic TACR No. TH02020057 "Program Epsilon".

This work has originated within the framework of the project TN01000007-NCE.

REFERENCES

1. C. Tropea, A. L. Yarin, and J. F. Foss, "Springer handbook of experimental fluid mechanics" (2007)
2. S. B. Pope, "Turbulent flows" (2000)
3. G. I. Ilieva, "A deep insight to secondary flows", Deflect and Diffusion Forum **379**, 83 – 107 (2017)
4. G. P. Romano "Large and small scales in a turbulent orifice round jet: Reynolds number effects and departure from isotropy", International Journal of Heat and Fluid Flow **83**, 108571 (2020)
5. S. Dutta, P. K. Panigrahi, K. Muralidhar, Journal of Engineering Mechanics **134**, 788 (2008)
6. M. K. Chauhan, S. Dutta, B. K. Gandhi, Journal of Wind Engineering and Industrial Aerodynamics **184**, 342 (2019)
7. J. L. Lumley, G. R. Newman, "The return to isotropy of homogeneous turbulence", Journal of Fluid Mechanics **82**, 161-178 (1977)
8. D. Duda, V. Uruba, "Spatial Spectrum From Particle Image Velocimetry Data", ASME J of Nuclear Rad Sci. **5**, 030912 (2019)